Structure
Article

Engagement of Arginine Finger to ATP Triggers Large Conformational Changes in NtrC1 AAA+ ATPase for Remodeling Bacterial RNA Polymerase

Baoyu Chen,[1,6,7] Tatyana A. Sysoeva,[1,6] Saikat Chowdhury,[1] Liang Guo,[2] Sacha De Carlo,[3] Jeffrey A. Hanson,[4,5] Haw Yang,[4,5] and B. Tracy Nixon[1,*]

[1]Department of Biochemistry and Molecular Biology, The Pennsylvania State University, University Park, PA 16802, USA
[2]BioCAT at APS/Argonne National Lab, Illinois Institute of Technology, 9700 South Cass Avenue, Argonne, IL 60439, USA
[3]Chemistry Department and Institute for MacroMolecular Assemblies, Marshak Science Building, City University of New York, NY 10031, USA
[4]Department of Chemistry, University of California at Berkeley, Berkeley, CA 94720, USA
[5]Department of Chemistry, Princeton University, Princeton, NJ 08544, USA
[6]These authors contributed equally to this work
[7]Present address: Howard Hughes Medical Institute and Department of Biochemistry, University of Texas Southwestern Medical Center, Dallas, TX 75390, USA
*Correspondence: btn1@psu.edu
DOI 10.1016/j.str.2010.08.018

SUMMARY

The NtrC-like AAA+ ATPases control virulence and other important bacterial activities through delivering mechanical work to σ54-RNA polymerase to activate transcription from σ54-dependent genes. We report the first crystal structure for such an ATPase, NtrC1 of *Aquifex aeolicus*, in which the catalytic arginine engages the γ-phosphate of ATP. Comparing the new structure with those previously known for apo and ADP-bound states supports a rigid-body displacement model that is consistent with large-scale conformational changes observed by low-resolution methods. First, the arginine finger induces rigid-body roll, extending surface loops above the plane of the ATPase ring to bind σ54. Second, ATP hydrolysis permits Pi release and retraction of the arginine with a reversed roll, remodeling σ54-RNAP. This model provides a fresh perspective on how ATPase subunits interact within the ring-ensemble to promote transcription, directing attention to structural changes on the arginine-finger side of an ATP-bound interface.

INTRODUCTION

Unlike the σ70-form of bacterial RNA polymerase, the σ54-form (Eσ54) cannot, on its own, melt double-stranded DNA and form an open complex to start transcription. This only happens after the stimulatory action of a *b*acterial *e*nhancer *b*inding *p*rotein (bEBP), which functions as a molecular motor belonging to the NtrC subclass of the extended family of AAA+ ATPases (Neuwald et al., 1999). Such ATPases are used in all cells to remodel macromolecules to perform a wide variety of cellular functions. For bEBPs the goal is to remodel the σ54 factor of Eσ54 to permit DNA melting and stabilization of open complexes (reviewed in Rappas et al., 2007; Tucker and Sallai, 2007). Because hundreds of bacterial species possess thousands of these activators, many having been shown to regulate nutrient acquisition, complex developmental pathways, and important virulence factors, it is important to understand the molecular basis of bEBP function.

AAA+ ATPases typically work as ring-shaped assemblies of identical subunits, with an active site residing at each interface between subunits. ATP contacts the Walker A and B motifs, Sensor I and Sensor II of one subunit (hereafter denoted "Walker-subunit"), and the arginine finger (Rfinger) of the apposing subunit (Rfinger subunit). For bEBPs, low-resolution EM and X-ray solution scattering studies suggest that ATP binding stabilizes extension of surface loops (hereafter denoted "L1-loops") so that their highly conserved "GAFTGA" motifs can bind to σ54 (Bose et al., 2008; Chen et al., 2007; De Carlo et al., 2006; Lee et al., 2003; Rappas et al., 2005). High-resolution structures of ATP-bound bEBP have remained elusive, with the only existing ones being derived from soaking crystals of apo-PspF with ATP (Rappas et al., 2006) or with ATP coincidentally present at one interface of otherwise apo-ZraR (Sallai and Tucker, 2005). In both structures the differences from other nucleotide states are small rather than large as suggested by the low-resolution data, and the Rfingers remain distant from the γ-phosphate of ATP unlike the tightly bound configuration typically seen for AAA+ ATPases (Thomsen and Berger, 2008). Here, we report the first bEBP crystal structure with Rfingers engaging ATP γ-phosphate. Comparing this new structure for the central domain of the NtrC1 ATPase of *Aquifex aeolicus* (hereafter denoted "NtrC1^{C}") with its previously determined ADP-bound one suggests rigid-body roll within subunits that is consistent with the large-scale changes seen in the low-resolution studies. A resulting model explains how interaction between Rfinger and ATP prepares the L1 loops for binding to σ54 and prepares the ATPase for remodeling the sigma factor. The model also suggests how neighboring subunits might communicate with each other.

RESULTS

Properties of Walker-B Mutant NtrC1^{C,E239A}

To obtain a crystal structure containing engaged Rfinger(s), we searched for an alanine substitution variant that binds ATP and σ54 but does not hydrolyze ATP or activate transcription. The Walker-B variant NtrC1^{C,E239A} was the only one identified with these properties (Figure 1; see also Figures S1 and S2 and Table S1 available online). Fluorescence polarization assays showed that NtrC1^{C,E239A} bound BODIPY-AMPPNP and ADP like wild-type protein. However, ATPase assays revealed that it was at least 150-fold less able to hydrolyze ATP. In response to ATP binding, NtrC1^{C,E239A} formed oligomers with the same Stokes radius as seen for NtrC1^{C,WT} when it binds the ATP ground-state analog ADPBeF$_x$. The ATP-bound NtrC1^{C,E239A} also formed complex with σ54 (Figures 1A and 1B). Small-angle X-ray scattering (SAXS) profiles of NtrC1^{C,E239A} in the APO state and in the presence of different nucleotides were very similar to those seen for NtrC1^{C,WT} (Figures 1C; Figure S1D). The resulting p(R) functions for the NtrC1^{C,E239A} data (Figure 1D) reveal two classes of solution structures, one for APO and ADP-bound states, and one for ATP or ATP analog-bound states. Comparing low-resolution structures derived from the scattering data with those for the wild-type protein showed that NtrC1^{C,E239A} underwent similar changes upon binding of ADP-BeF$_x$, ATP or ADP-AlF$_x$ (Figure 1E). These changes include loops extending above the pore of the ring, overall ring shrinkage, and spike formation on the outer periphery of the ring. However, unlike the wild-type protein, the E239A variant did not activate transcription (data not shown). Collectively, these observations showed that although the Walker-B mutant is not able to hydrolyze ATP or activate transcription, it does bind ATP, and that stabilizes conformations that bind to σ54.

Crystal Structure of NtrC1^{C,E239A} Identifies R299 as the Rfinger in a Heptameric Closed Ring

An ATP-bound NtrC1^{C,E239A} structure was refined to 2.63 Å using data from rod-shaped crystals grown in space group $P2_12_12$ in the presence of 20 mM $MgCl_2$ and ATP (Table 1; PDB code 3M0E). A closed-ring heptamer containing a high degree of non-crystallographic symmetry was present in each asymmetric unit (Figure 2A). Visual inspection and final NSD superpositioning values (Kozin and Svergun, 2001) showed that the structure fit best to the SAXS models for ATP- or analog-bound states rather than ADP or APO states (Figures 1E; Figure S1E). The L1 loops containing the conserved GAFTGA motifs that physically bind σ54 lay above the plane of the ring, pointed toward the central pore. Resolve maps (Terwilliger, 2000) showed unbiased electron density for most of the backbone of the L1 loops (Figure 2B), but some residues were associated with high B factors and weaker electron density indicative of flexibility in the GAFTGA-motif portion of these loops. Prime-and-switch, resolve, and simulated annealing omit maps built from the model lacking nucleotide showed strong density for ATP and Mg^{2+} in each active site (Figure 2C).

Based on sequence analyses and existing structures, bEBPs have two candidates that could be the Rfinger (R299 and R293 in NtrC1); the new structure shows the NH1 and NH2 atoms of R299 clearly engaged with the γ-phosphate of ATP that is bound across the interface to the adjacent subunit's Walker and Sensor motifs (Figure 2C). In agreement with this assignment, purified NtrC1^{C,R299A} variant bound nucleotides but failed to undergo nucleotide-dependent conformational changes, to hydrolyze ATP and to bind σ54. Variant NtrC1^{C,R293A} formed less stable

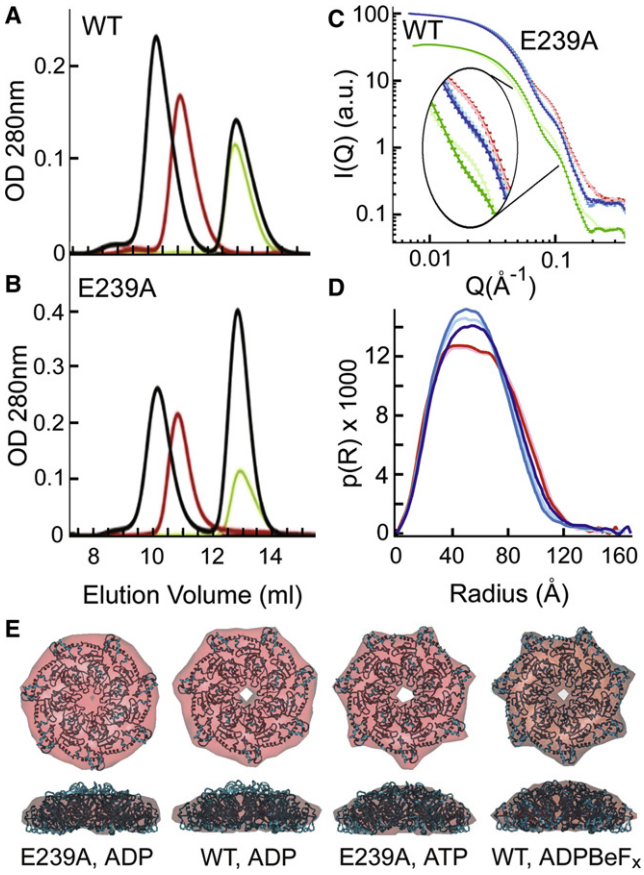

Figure 1. Properties of Amino Acid Variant NtrC1^{C,E239A}

(A) Size-exclusion chromatography profiles illustrate the ability of NtrC1^{C,E239A} to self-assemble and to bind to σ54 in the presence of Mg/ATP. Elution profiles are shown for ATPase alone (green), ATPase with nucleotide (red), and ATPase plus excess σ54 with nucleotide (black). SDS-PAGE analyses (not shown) confirmed the co-elution of both proteins in the complex peak (black arrow).

(B) Control experiments with NtrC1^{C,WT} using the ATP-transition state analog ADPAlF$_x$.

(C) Solution X-ray scattering profiles (arbitrary intensity scale versus momentum transfer Q) of different nucleotide states of NtrC1^{C,E239A} (upper curves: APO, pink; Mg/ADP, red; Mg/ADPBeF$_x$, cyan; Mg/ADPAlF$_x$, medium blue; Mg/ATP, dark blue) and NtrC1^{C,WT} (lower curves: APO, light green; Mg/ADPAlF$_x$, dark green) reveal similar conformational changes for wild-type and mutant protein. For clarity, data for NtrC1^{C,WT} are offset by −0.8 a.u., and the enlargement shows the high precision of the data: each horizontal bar being ± standard error.

(D) Distance distribution function p(R) for scattering data from NtrC1^{C,E239A} (same colors as in C). R_g and D_{max} values from these distribution functions are: 45.7 ± 0.1 Å, 136 Å; 45.4 ± 0.1 Å, 136 Å; 43.3 ± 0.1 Å, 129 Å; 42.8 ± 0.1 Å, 127 Å; 45.1 ± 0.1 Å, 135 Å for NtrC1^{C,E239A}; and 47.5 ± 0.1 Å, 142 Å; 43.8 ± 0.1 Å, 135 Å for NtrC1^{C,WT}.

(E) Ab initio solution structures (transparent red envelopes) for the NtrC1^{C,E239A} or NtrC1^{C,WT} superimposed on the new crystal structure of ATP-bound NtrC1^{C,E239A} (ribbons; final NSD values: E239A: ADP 1.625 ATP 1.224; and WT: ADP 1.487, ADPAlF$_x$ 1.262). See also Table S1 and Figures S1 and S2.

Table 1. Data Collection and Refinement Statistics

	$NtrC1^{c,E239A}$[a]
Data Collection	
Space group	$P2_12_12$
Cell dimensions	
—*a*, *b*, *c* (Å)	40.70, 242.59, 251.21
Resolution (Å)	47.64–2.63 (2.72–2.63)[b]
R_{merge}	9.1 (48)
$I/\sigma I$	9.7 (1.8)
Completeness (%)	99.7 (83.3)
Redundancy	7.9 (4.78)
Refinement	
Resolution (Å)	47.64–2.63
Number of reflections	75,935
R_{work}/R_{free}	20.5/23.9
Number of nonhydrogen atoms	
—Protein	13,827
—ATP	217
—Magnesium	7
—Water	391
B factors	
—Protein	53.8
—ATP	43.3
—Magnesium	51.3
—Water	48.5
Rms deviations	
—Bond lengths (Å)	0.009
—Bond angles (°)	1.25

[a] One crystal was used for the data collection.
[b] Values in parentheses are for the highest resolution shell.

rings and showed reduced ATP hydrolysis, but it still changed conformation upon nucleotide binding, bound to σ54 and activated transcription (Table S1).

Most AAA+ ATPases function as hexamers, although other stoichiometries have been observed. $NtrC1^{C}$ forms heptamers both in solution (Chen et al., 2007) and in prior ADP-bound (Lee et al., 2003) and now ATP-bound crystal structures. We used negative-stain EM to confirm that the heptamer rings of $NtrC1^{C,WT}$ bind σ54. Random-conical tilt (Radermacher et al., 1987) was used to build a low-resolution three-dimensional model from 9000 images of the $NtrC1^{C,WT}$-σ54 complex. Although a significant portion of the density for σ54 was missing from the modeled structure, comparing projections of the $NtrC1^{C,WT}$ ring alone and its complex with σ54 (Figure S3) showed that heptamers bind the sigma factor.

Comparing ATP- and ADP-Bound $NtrC1^{C}$ Structures Reveals Large-Scale Conformational Changes

We next compared the new ATP-bound structure of $NtrC1^{C,E239A}$ with the previously reported ADP-bound one for $NtrC1^{C,WT}$. Superimposing the two structures using just their nucleotide-binding P loops (residues 168–175; Figure 3A) or using a maximum likelihood approach (Theobald and Wuttke, 2008) (data not shown) suggested that the presence of the γ-phosphate of ATP stabilized a large displacement of the L1 and L2 loops. This corresponds to the loops of the ATP-bound state being more extended above and away from the plane of the ring (Figure 2A, side view). The underlying basis for this displacement was revealed by distance difference matrix analysis (Mosca and Schneider, 2008a, 2008b) of chain A of the ATP-bound structure with the 14 non-symmetry related chains of the ADP-bound structure. The analysis defined two rigid bodies and two flexible regions (Figure 3B). The first flexible region is the GAFTGA motif itself, whose flexibility is reflected in high B factors and weak electron density. The second flexible region, which has significantly stronger electron density, includes the N-terminal 2/3 of helix H10 (residues 242–247 and 250–252). The cleft between the larger rigid body (colored white in Figure 3C) and smaller rigid body (colored blue) is more open in the ATP-bound state. These results were consistent with the output of Dyndom (Hayward and Berendsen, 1998), which, using an alternative algorithm, identified clusters of rotation vectors indicating a 10°–13° rotation of the L1 and L2 loops with respect to the rest of the subunit (data not shown). None of the other bEBP structures has engaged Rfingers, and similar pair-wise comparisons of their subunits failed to reveal any such motions.

ATP Binding Reorganizes Subunit/Subunit Interface

To understand the basis for the large-scale rigid-body displacement, we compared the new ATP-bound, Rfinger-engaged subunit interface with that previously determined for the ADP-bound, Rfinger-disengaged structure. This comparison revealed significant reorganization of the interface between subunits, with changes seen in four groups of interactions, three being unique to the ATP-bound state (Figure 4; Table S2 lists potential H bonds in both the ADP- and ATP-bound states). The first group of interactions surrounds the Rfinger and γ-phosphate of ATP (Figure 4B), where helix H11 containing the Rfinger of the Rfinger subunit contacts the γ-phosphate of ATP, Sensor II helix (H14), Sensor I, and the tip of the Walker-B β strand of the Walker-subunit. Mg^{2+} is coordinated by both β- and γ-phosphate oxygen atoms, in contrast to the $PspF^{C,R227A}$ structure of APO-grown crystals soaked in Mg^{2+}/ATP (PDB 2C9C) (Rappas et al., 2006), where it is coordinated by the α- and γ-phosphate and shifted by 3 Å. R357 on Sensor II of the Walker-subunit contacts the α- and γ-phosphates of ATP, with the R357 NH2 atom located where Mg^{2+} is modeled in the PspF structure. Rfinger and γ-phosphate interactions are buttressed by inter-subunit contact between D295 of the Rfinger helix and N280 of Sensor I, and intra-subunit contact between D295 and R293. R293 also contacts E242 at the end of the Walker-B β strand or beginning of Linker 2 (labeled in Figures 3A and 4B).

The second group of interactions links helix H9 of the Rfinger subunit with the Walker A and B motifs of the Walker-subunit (Figure 4C). These interactions include contacts between R253 of helix H9 and E174 and D238 from Walker A and B across the interface. E174 clearly coordinates with the Mg^{2+} ion, and D238 is within 4 Å. The missing side chain of Walker-B residue E239 can readily be modeled to contact R293 of the Rfinger subunit, or contact N280, D238, or N195 of its own protomer. The third group (Figure 4D) involves the hydrophobic portion of

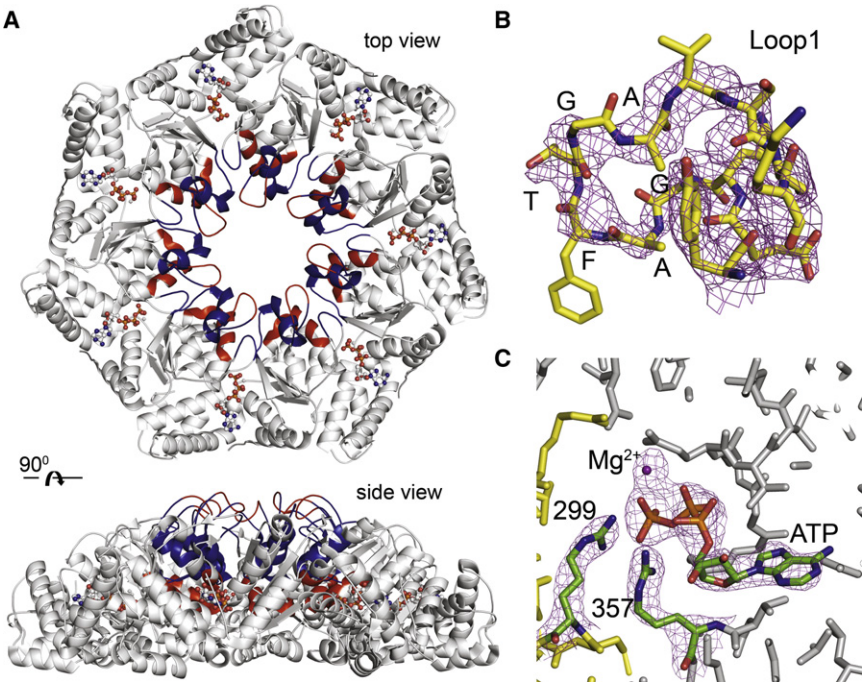

Figure 2. Mg^{2+}/ATP-Bound, Rfinger-Engaged Structure of $NtrC1^{C,E239A}$

(A) Top and side views of heptamer ring. Two rigid bodies (white, rigid-body 1; blue, rigid-body 2) and two flexible regions (red; see text and Figure 3) are symmetrically ordered with Mg^{2+}/ATP bound at the cleft between protomers.

(B) Resolve density map and final model of the GAFTGA motif of chain A contoured at 2.4 sigma.

(C) Simulated anneal density map calculated with model lacking Mg^{2+}/ATP, contoured at 5 sigma. The ATP and Mg^{2+} ion were added after map calculation. Contact with the γ-phosphate of ATP is illustrated for the Rfinger (R299) and the arginine of Sensor II (R357), the latter of which also contacts the α-phosphate.

Conformational Changes Propagate from Rfinger to σ54-Binding L1 Loops

The ATP-imposed reorganization of the subunit interface described above was also associated with an intriguing network of changes in secondary structural elements and side chain locations that propagate away from the engaged Rfinger (Figure 5A). Importantly, a direct path for this propagation runs from engaged Rfinger through atoms supporting the rigid-body roll within the Rfinger-engaged subunit rather than within the Walker-subunit. Bound ATP provides a γ-phosphate for stabilizing the Rfinger of helix H11 in its "engaged" orientation (labeled "R299" in the side chain of K250 of helix H9 of the Rfinger subunit and S198 and P200 in Linker 1 of the Walker-subunit. The fourth group (Figure 4D), also seen in most ADP-bound interfaces, "glues" the L2 loop of the Rfinger subunit with the L1 loop of the Walker-subunit by hydrophobic interactions between Y261 and R266 of the former and F226 and L229 of the latter.

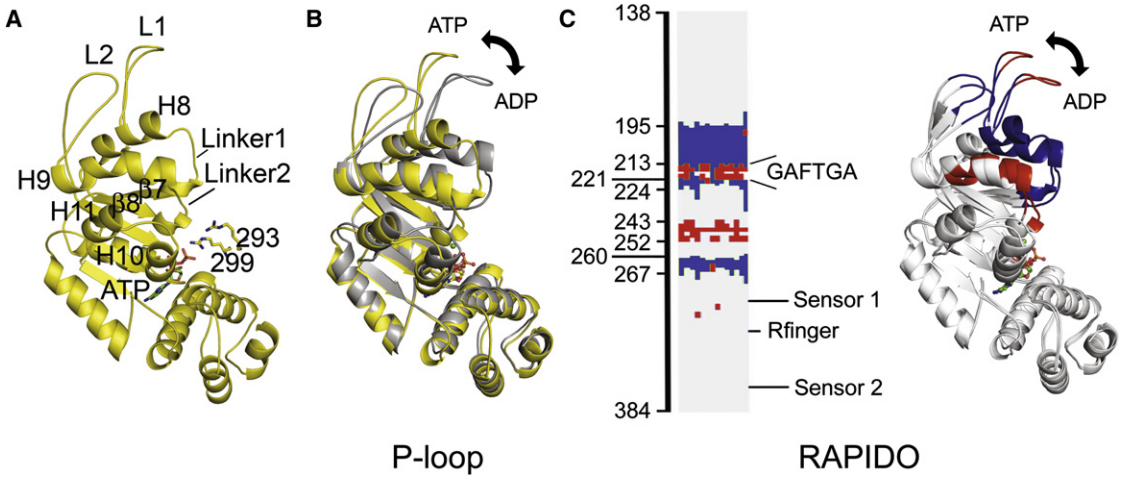

Figure 3. Relative Displacement between ATP- and ADP-Bound Subunits

(A) To the left, a single protomer is shown identifying important structural elements (the L1 loop contains the GAFTGA motif; the Rfinger residue R299 and residue R293 are from the otherwise not shown, adjacent protomer; and secondary structure elements are numbered as in the structure for $NtrC1^{RC}$, PDB code 1NY5, which contains both N-terminal receiver and central ATPase domains).

(B) ATP-bound (yellow) and ADP-bound (gray, chain A, PDB 1NY6) models aligned on P-loop residues 168–175. Arrow denotes displacement between ATP and ADP bound states.

(C) To the left, each column portrays the difference distance matrix assignments from RAPIDO for the ATP-bound structure compared to one of the 14 ADP-bound subunits. Collectively, they assign: rigid-body 1 (off-white, defined as residues 138–194, 225–241, 253–260, 267–384); rigid-body 2 (blue, defined as residues 195–213, 222–224, 261–266); flexible region 1 (red, residues 214–221); and flexible region 2 (red, residues 242–247, 250–252). To the right, ATP-bound and ADP-bound models are aligned on rigid body 1. Arrow denotes rigid-body roll between ATP and ADP bound states. See also Figure S2.

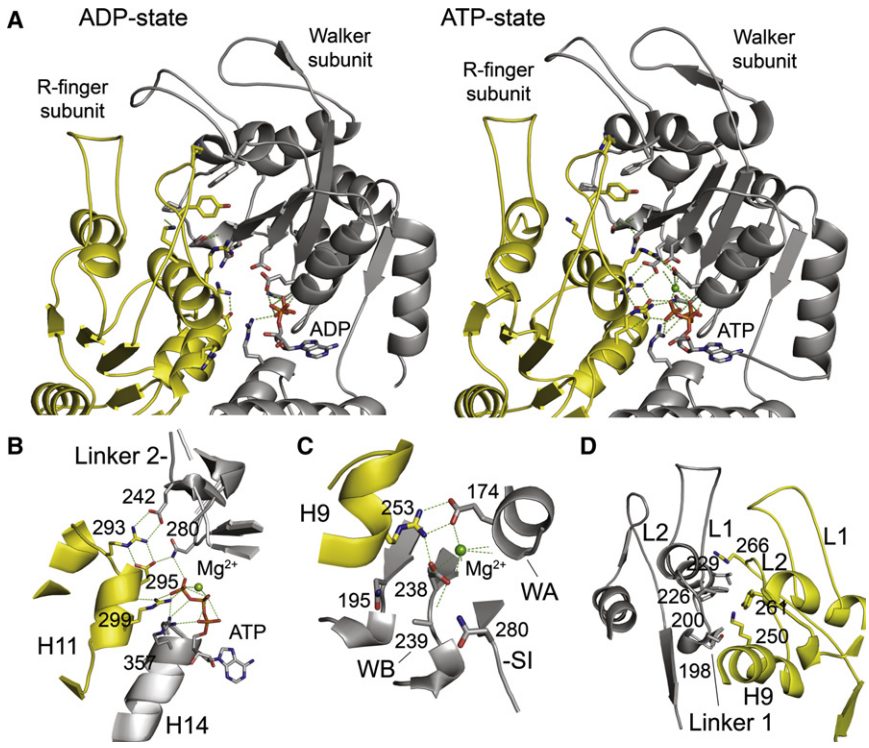

Figure 4. ATP-Driven Reorganization of the Subunit Interface

(A) ADP- and ATP-bound interfaces between two subunits. Walker-subunit is colored gray and Rfinger-subunit yellow.

(B) Close-up of the active site occupied with ATP showing contacts from the R-finger group. Potential hydrogen bonds are shown as dashed green lines.

(C) Interactions of the R253 residue at the ATP-bound interface. Below are residues surrounding A239.

(D) The L1-GAFTGA and L2 interface (rotated 180° relative to A–C): two clusters of interactions reside above the active site. Those of group four are in front at the bottom: residues S198 and P200 on the Walker-subunit with K250 on the Rfinger subunit. Those of group four are in back at the top: residues F226, L229 on the Walker subunit, with Y261 and R266 on the Rfinger subunit. See also Figures S2 and S4.

Figure 5B). This entails inserting the hydrophobic backbone of the Rfinger side chain into an i ± 4 groove formed by E256 and V252 on neighboring helix H9 (Figure 5B). In order to accommodate the inserted Rfinger side chain, the trajectory of H9 is stabilized in a distorted and extended helical conformation, perhaps influenced by interaction between R253 and Mg^{2+}. In this extended state a hydrophobic groove between K250 and V254 accommodates the tip of F209 so that it is rotated a few degrees relative to its position in the ADP-bound subunit (Figure 5C). This rotation reorients a highly conserved hydrophobic cluster formed by F209, F227, F260, V254, L263, and the hydrophobic portions of the side chains of E205, E212, and R262 (Figure 5D). The cluster abuts the base of the stem from which the L1 loop containing the GAFTGA motif emerges, the L2 loop, helix H9, and a neighboring cluster of hydrophobic and electrostatic contacts between L1 and L2 loops (residues R262, E212, and S222). In addition to staging this hydrophobic foundation for rigid-body roll, the distorted helix H9 favors it by promoting reorientation of side chain charges from K250 and E246 to form a charge cluster with E205 and R201 of the N-terminal end of helix H8 just prior to the beginning of the stem of the L1 loop (Figure 5E). This electrostatic cluster seems to stabilize an unwinding of the first turn of helix H8 and substantial relocation of the preceding loop, Linker 1 (Figure 5D). Further stabilization of these changes comes from contact between E242 at the base of Linker 1 and R293 of the neighboring subunit (Figures 4B and 5E). Finally, within the Rfinger-subunit V252, A249, Q248, and L245 (Figure 5E) sandwich the hydrophobic portion of R293 and interact with F292 to help position helix H10, which may communicate with the DNA-binding domain that would be located immediately below were it to be present (inferred from De Carlo et al., 2006).

Steric-Clash between Components of ATP- versus ADP-Bound Interfaces

The interactions just described for an ATP-bound interface stabilize a closer juxtaposition of the two subunits than is present in any of the 14 ADP-bound interfaces. This tighter interface has several implications. From the perspective of the Walker-subunit (colored gray in Figures 4 and 6), strand-β8 (Walker-B) and strand-β7 have to shift their respective equilibrium positions in order to avoid steric repulsion. Importantly, it requires a much larger relocation of the ensuing loop, Linker 1, which in this alignment is as much as 7.5–8.0 Å displaced from its position in the ADP-bound state (Figures 3B, 3C, and 6). Movement of Linker 1 is associated with partial unwinding and relocation of helix H8, which is accompanied by outward extension of the L1 loop. With the L1 loop being tightly associated with the supporting L2 loop (Figures 5A and 5D), L1 movement is joined by movement of L2, and of helix H9, which abuts the Walker A and B motifs of the Walker-subunit (Figure 6). L1 and L2 loops of adjacent subunits are also tightly bound via a set of unchanged contacts present in both ADP-bound and ATP-bound subunits, as described above (Figure 4D). Given these tight connections and the symmetry of this ATP-saturated structure, these conformational arrangements propagate through each subunit of the ring.

Properties of Substitutions in Canonical AAA+ ATPase Residues and K250E

The effect of alanine substitutions in key AAA+ ATPase residues Walker A (K173), Walker-B (D238, and see above for E239), Sensor I (N280), Sensor II (R357), and glutamate switch (N195) gave results consistent with those already published for PspF and other bEBPs (Table S1 and Figure S2). Except K173A, which binds nucleotide very weakly, all mutant proteins were able to bind ATP but largely or completely ineffective in hydrolyzing it. Like the Rfinger substitution R299A, those in D238 and R357

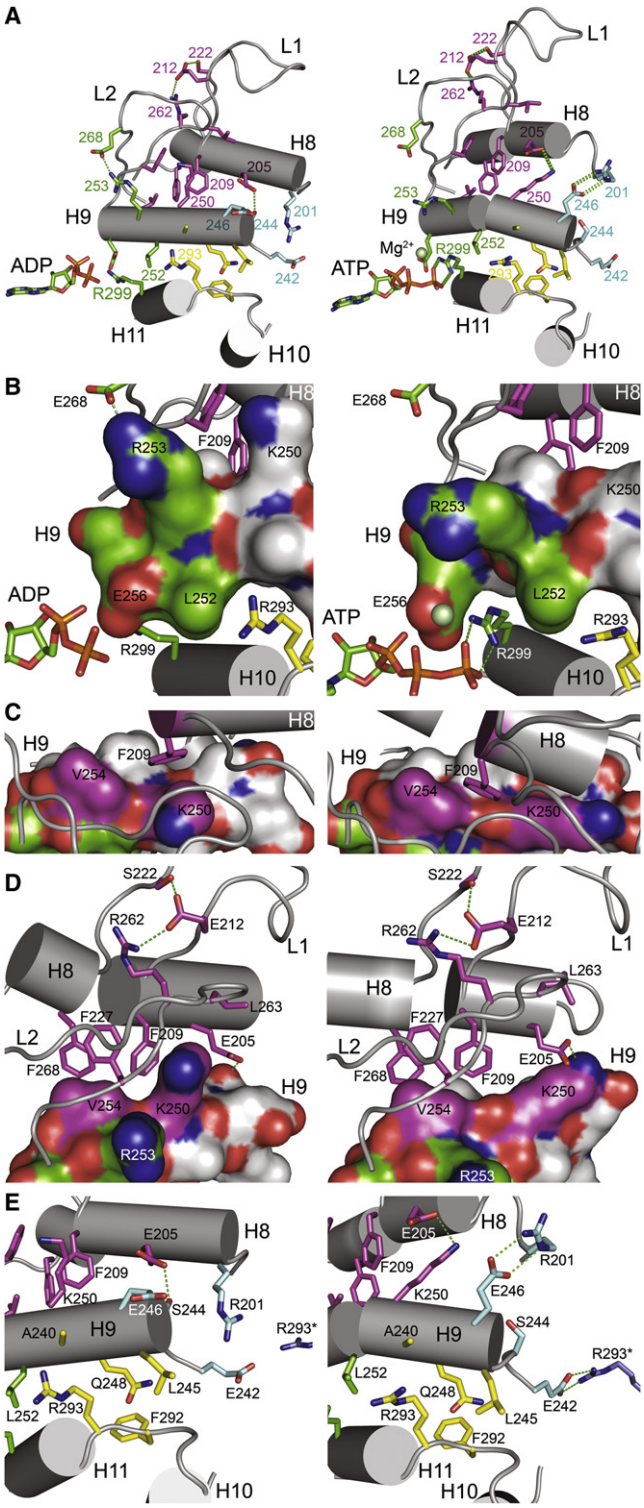

Figure 5. Conformational Change Propagating from the Engaged Rfinger

ADP-bound structures (left) are aligned to ATP-bound structures (right) on rigid-body 1.

(A) Four groups of interactions (see text) are shown in green, magenta, cyan, and yellow viewed from the Walker-subunit side of an interface near the pore of the ring and looking at the Rfinger subunit.

(B) Rfinger (R299) inserted into i ± 4 groove of helix H9 formed by E256 and L252 to engage γ-phosphate of ATP.

(C and D) (C) Top view from L1 to H9 in (A) showing that relocation of the side chain of K250 accommodates rotation of F209: the basal tip of rigid-body 2 maintained by hydrophobic and charge interactions that are conserved between ADP and ATP states, shown in (D).

(E) Kink in helix H9 and relocation of the K250 side chain redefine the charge cluster between N-terminal ends of helixes H8 and H9, stabilizing unwinding and rolling of H8 (top), and also pushing helix H10 downward via a stable group of hydrophobic interactions (yellow residues). See the Supplemental Movie "NtrC1C_engine.mov" for a stereo rendition of the transitions from presumed APO to ATP-bound and ATP-bound to ADP-bound states for binding and then remodeling σ54, and Figures S2 and S4.

failed to undergo SAXS-defined conformational changes upon binding nucleotide; both could not hydrolyze ATP or activate transcription and only showed limited ability to bind to σ54. Substitution N280A interacted poorly with σ54 except in the presence of ADPAlF$_x$ and showed reduced ability to activate transcription. Only substitution N195A showed normal conformational changes induced by ATP or ATP-analog binding and ability to bind σ54, but it too had a reduced ability to hydrolyze ATP and activate transcription.

Previous interpretations of such phenotypes have focused on potential structure/function effects on the Walker-subunit. The set of structural changes we describe between the ATP- and ADP-bound ATPase suggested that key residues of the Rfinger subunit play important roles in the conversion of ATP binding and hydrolysis into mechanical work on σ54. Strikingly, the side chain of K250 appears to exist in distinct environments in the two nucleotide-bound states (Figures 5A and 5C–5E; Movie S1), from where it alternately contributes to stabilizing both end points of the observed rigid-body roll. As an initial test of its functional importance, we substituted K250 with glutamate to determine if the ATPase depends upon the positive charge of this conserved residue. Gel filtration experiments showed that the K250E variant was partially impaired but still able to assemble rings and bind to σ54 when provided Mg^{2+} and ADPAlF$_x$ (Figure 7A) (similar results for ADPBeF$_x$ are not shown). SAXS data, collected at 10-fold higher protein concentration, showed apparently complete ring assembly in APO, Mg/ADPBeF$_x$, or Mg/ADPAlF$_x$ states (Figure 7B). Unlike the wild-type protein, the K250E variant bound to ADPAlF$_x$ was larger than when bound to ADPBeF$_x$. Models derived assuming homogeneity and 7-fold symmetry (yet to be established for the mutant protein) suggested that both ADPBeF$_x$ and ADPAlF$_x$ analogs supported an extended loops state, but the loops' extension with ADPAlF$_x$ was unusually pronounced (Figure 7B). The K250E variant precipitated upon the addition of Mg^{2+}/ADP but completely redissolved upon further addition of AlF$_x$ or BeF$_x$ complex ions, converting the ADP to ATP analogs (Figure 7C). We infer that the K250 side chain is in fact located in significantly different environments in ADP- and ATP-bound states and that this residue's positive charge is important for ATPase assembly and conformational response to ATP.

DISCUSSION

The structure we report describes a prehydrolysis state of the bEBP catalytic cycle that has previously eluded detection. It

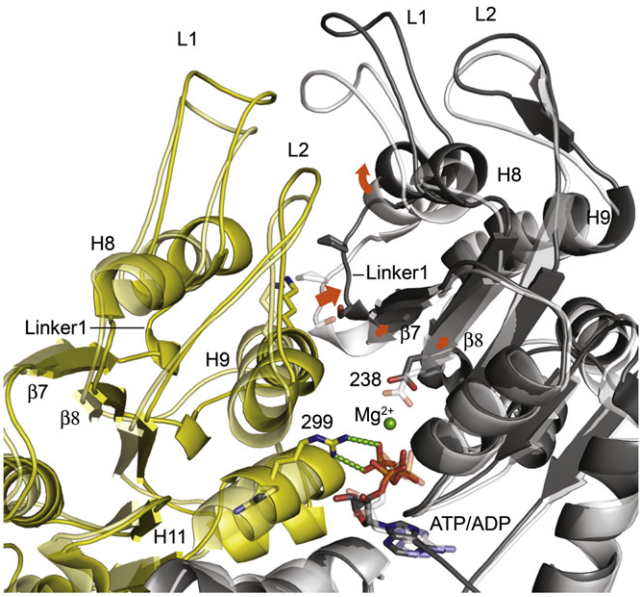

Figure 6. Communication of Rfinger-Subunit's Engaged Status to Adjacent Walker-Subunit

Rfinger (labeled "299") engages the γ-phosphate of ATP, promoting a tighter interface and structural rearrangements between two subunits (Walker-subunit, gray; Rfinger subunit, yellow; the ADP state is represented by the same colors, but transparently). The Walker-subunit is superimposed on rigid-body 1 of an ADP-bound subunit. Also labeled are the secondary structure elements Linker 1, helixes H8, H9, and H11, L1 and L2 loops, and strands β7 and β8. Movement induced in the Walker-subunit (red arrows) in strand β7 and Linker 1 is associated with partial unwinding and translocation of helix H8, and with an upward and outward roll of the L1 loop and its σ54-binding GAFTGA motif. The tightly connected Loop L2 is accordingly moved right, with its supporting helix H9 and preceding linker slightly pressed downward.

provides the first detailed description of a subunit/subunit interface for the ATP-bound, Rfinger-engaged stage of a closed ring. Comparing it with available bEBP structures let us formulate a rigid-body displacement hypothesis that explains how ATP binding and hydrolysis could be associated with conformational changes to perform mechanical work on Eσ54. The hypothesis suggests that (a) within the Rfinger subunit, key residues and secondary structural changes relay engagement of the Rfinger with the ATP γ-phosphate to the distant σ54-binding GAFTGA-motif in the L1/L2 rigid body; and that (b) changes in the two interfaces of the Rfinger-engaged subunit propagate its status to neighboring subunits in the ring.

We discuss this model, summarized in Figure 8 and Movie S1, by first describing interactions between subunits and then focusing on the context of a closed-ring of subunits. The glutamate-switch hypothesis (Zhang and Wigley, 2008) describes what might happen when ATP first binds to a bEBP: the Walker-B glutamate of the Walker-subunit rotates away from its catalytic position and engages with a nearby asparagine. This conformation disables the glutamate from activating water as a nucleophile, thus preventing hydrolysis. Based on the new structure, we suppose that across the interface the Rfinger-subunit's Rfinger changes from interacting with its apposing Walker-B subunit's Sensor II helix to engage with the γ-phosphate of the interface-bound ATP. To provide a groove for the Rfinger to project toward the γ-phosphate, a kink is formed in the overhanging α-helix H9 of the Rfinger subunit. This kink also provides a second hydrophobic groove on the distal side of the helix and positions the helix's side chains to permit and to stabilize a 10°–15° roll of a small rigid body, moving the L1 and L2 loops and, as a consequence, the σ54-binding GAFTGA motif away from the surface of the ring. When subsequent ATP hydrolysis converts the γ-phosphate to free P_i the Rfinger is no longer tethered. It is thus released to return to its location near the Sensor II helix of its interface partner subunit, triggering relaxation of the kinked helix and reversal of the rigid-body roll that is used to perform mechanical work on σ54.

This new model sheds light on how subunits communicate throughout a functioning ring. Given the intrinsic incompatibility of the ATP- and ADP-bound interfaces and the tight linkage between L1 and L2 loops, rigid-body roll subsequent to ATP binding to one subunit would tend to be propagated throughout the ring. In a functioning ATPase the extent of such propagation would likely depend strongly upon the presence or absence of γ-phosphate in neighboring interfaces. One could suppose, for example, that a subunit with engaged Rfinger is most functional when its Walker face is not bound to ATP because occupancy would cause the neighboring subunit to also be in an extended loops conformation. Having both subunits favoring such a conformation would cause a push from the tightly linked L2 and L1 loops across the interface and steric clash with Linker 1 that would oppose the return roll of the rigid body of L1 and L2 loops and, thus, diminish the ability to deliver force to the σ54-form of RNAP. If a subunit experienced hydrolysis and Rfinger retraction, its tendency to roll into the ADP-bound structural state may well be opposed by an ATP-bound neighbor on the other side as well. Although ATP might be hydrolyzed, conformational change and product release could be delayed, slowing down the catalytic cycle. Such hypothetical events offer a mechanism for how nucleotide status at neighboring interfaces effects negative cooperativity for catalysis that was proposed to explain why high concentrations of ATP inhibit the rate of hydrolysis, whereas the addition of ADP stimulates it (Joly et al., 2006; Schumacher et al., 2008). Furthermore, SAXS data from titrations of metal fluoride analogs and time-resolved SAXS measurements monitoring changes after mixing analog and $NtrC1^C$ ATPase show a concentration-dependent, biphasic interaction with nucleotide that is associated with separate conformational changes in each phase (T.A.S. and B.T.N., unpublished data). An alternative explanation that is not mutually exclusive is that an ATP-occupied interface that flanks variable length runs of ATP-occupied interfaces acts as a dam, preventing rigid-body roll into the ADP-occupied state for the entire series of subunits until the dam breaks via hydrolysis at the boundary interface. In this way a randomly concerted mechanism might deliver variable strokes of force to remodel Eσ54. Such a mechanism may also be indifferent to precise stoichiometry in the ring, so long as changes from hexamer to heptamer can readily be adjusted (e.g., by small changes in the juxtaposition of α/β and α-helical subdomains) to permit formation of the proper working interfaces frequently enough for function to occur.

There are several strengths and some weaknesses of this model. First, it is consistent with estimated-likelihood statistical-coupling analysis (Dekker et al., 2004) of the bEBP PFAM

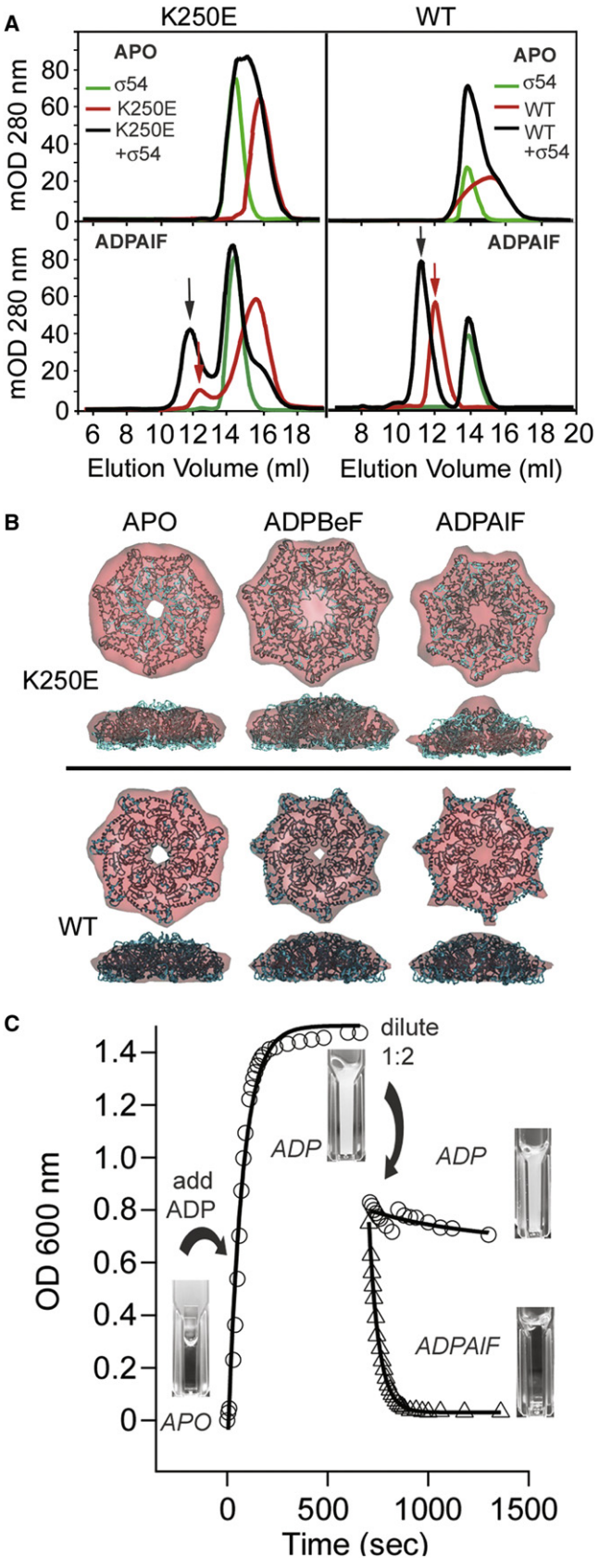

Figure 7. Properties of Substitution K250E

(A) Ring assembly and complex formation assayed by gel filtration for APO protein (top panels: K250E left, WT right) and protein incubated in the presence of Mg^{2+}/ADPAlF$_x$ (lower panels). Assembled rings elute at ~12 ml (red arrow), and complexes elute at ~11 ml (black arrow). Samples are ATPase alone (red), σ54 alone (green), and a mixture (black, 7:2 ATPase:σ54). Similar data, not shown, were seen for Mg^{2+}/ADPBeF$_x$.

(B) Filtered average of 50 ab initio GASBOR models from SAXS data measured for K250E (top) and WT (bottom) protein at 7 mg/ml concentration in APO, Mg^{2+}/ADPBeF$_x$, and Mg^{2+}/ADPAlF$_x$ states (red) superimposed on ATP-bound crystal structure of NtrC1^{C,E239A} (blue). From top left to bottom right, R_g and D_{max} values from the p(R) functions were: 43.9 ± 0.1 Å, 129 Å; 41.8 ± 0.1 Å, 127 Å; 48.3 ± 0.1 Å, 151 Å; 46.6 ± 0.1 Å, 142 Å; 42.0 ± 0.1 Å, 134 Å; and 42.5 ± 0.1 Å, 135 Å.

(C) Light scattering and images of cuvettes containing translucent or turbid solutions show precipitation of K250E upon addition of Mg^{2+}/ADP (1 mM): circles, first 700 s. Diluting 1:2 with 2× Mg^{2+}/AlF$_x$ (triangles) but not buffer (circles, second 700 s) brought the protein back into solution. Diluting with 2× Mg^{2+}/BeF$_x$ had the same affect (not shown).

family (9700 sequences) (Figure S4). This method, good at identifying residues with close physical proximity, predicts the interacting pairs K250/E205, R201/E246, and E174/R253 that we report are unique to the Rfinger-engaged, ATP-bound structure. The model is also consistent with structures of ZraR and PspF. The ZraR structure is of "apo" protein, in that no nucleotides were added before or after crystallization. For 2 of its 12 interfaces, there was density described as being possibly due to ATP at low occupancy and sulfates or possibly phosphates located in the remaining interfaces that were suggested to indicate where β-phosphate might reside. None of the subunits had engaged Rfingers, which are also absent in all PspF structures, regardless of the nucleotide-bound status. Thus, all of these structures are consistent with the current model, in total representing the following states: APO, ADP-bound, ATP-bound with glutamate-switch on and Rfinger disengaged, and ATP-bound without glutamate-switch but with Rfinger engaged. Finally, the model is also consistent with recent studies of PspF where two networks of residues were found to be important for substrate binding and transcription activation (Joly and Buck, 2010). These correspond to NtrC1 residues E212, S222, E228, and R262, or residues F226, L229, and Y261 (Figure S3). As described (Joly and Buck, 2010; and here), the first group tightly links L1 and L2 loops within a single subunit, whereas the second mediates contact between L2 and L1 loops in neighboring subunits. In PspF the latter involve electrostatic interactions, whereas in NtrC1 the interactions are hydrophobic in nature—in both proteins they could mediate rigid-body roll in the Rfinger subunit and its propagation to neighboring subunits. The phenotypes observed for these mutations could arise from softening the rigid body or diminishing repulsive or attractive interactions between the subunits and, thus, weaken the delivery of force to σ54.

The new ATP-bound structure is of a variant whose Walker-B glutamate has been substituted with alanine, raising the possibility that the substitution has stabilized a functionally irrelevant off-pathway state. Although possible, it could also be that removing the Walker-B glutamate accomplishes essentially the same inhibition of hydrolysis that was proposed for the glutamate switch (Zhang and Wigley, 2008) but irreversibly and,

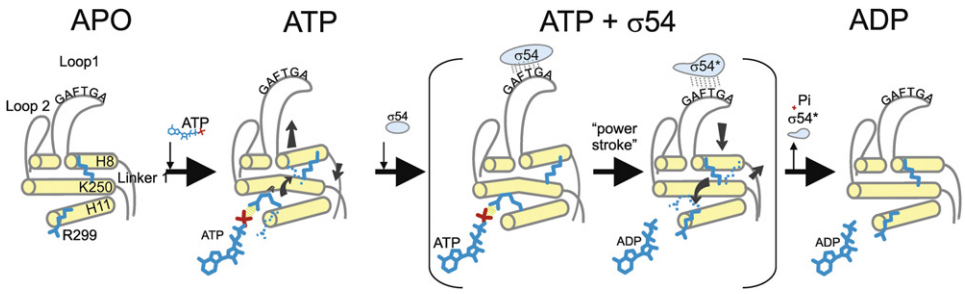

Figure 8. Schematic Model of Hypothetical Motor Mechanism

Conformational changes induced in the Rfinger subunit upon engagement with the γ-phosphate of ATP, its hydrolysis, and Pi release. Upon binding ATP, the Rfinger engages γ-phosphate, kinking helix H9 and permitting rigid-body roll of L1/L2 that extends GAFTGA motif for binding to σ54. Upon binding σ54 and the power stroke associated with hydrolysis, return of the Rfinger to its resting position, and Pi release, the sigma factor is remodeled (σ54*) so that promoter opening can occur.

thus, allowing capture of the Rfinger-engaged state. Because little conformational change other than the rotamer switch was seen in the ATP-soaked, APO-grown crystals of PspF that gave rise to the hypothesis (Rappas et al., 2006), the proposed hydrolysis-inhibiting action may result from predominantly local effects that are readily mimicked by substituting the Walker-B glutamate with alanine. Alternatively, if engaging the Rfinger is required to help the active site enter a transition state for hydrolysis, then hydrolysis may be delayed until after such engagement, and the role of the "glutamate-switch" may reside in as yet unknown but later aspects of the cycle. This is consistent with the properties of $NtrC1^{C,N195A}$ (and with many of the properties of N64 substitutions in PspF; Joly et al. [2008]), in which the glutamate switch is impossible, and yet the protein responds as WT to the binding of ATP until the step of hydrolysis.

Another point that warrants further discussion is whether study of the closed heptamer ring accurately reflects the functional basis of full-length bEBP in the context of its complexes with enhancer DNA and Eσ54 bound to promoter DNA. ATPase activity of bEBPs is typically regulated by controlled self-assembly into ring forms, which in structural studies have varied from spiral hexamers to closed-ring hexamers or heptamers (Batchelor et al., 2009; De Carlo et al., 2006; Lee et al., 2003; Rappas et al., 2005; Sallai and Tucker, 2005). For the NtrC1 ATPase domain, its crystal structures are heptameric (Lee et al. 2003 and this report), but class averages from negatively stained EM images revealed that it exists in solution as a mixture of 90% heptamers and 10% hexamers (Chen et al., 2007). In this report we show by EM that the heptamer form is functional in binding σ54. We also note that preparations known to be largely heptamers are quantitatively capable of forming complex with σ54, and they hydrolyze ATP and interact with Eσ54 both in vivo (Doucleff et al., 2005) and in vitro (this report) to form open complexes and activate transcription. Similarly, electrospray ionization mass spectrometry revealed heptamer rings for the related protein NtrC4, also of *A. aeolicus*, when the isolated ATPase domain or that attached to dimer-forming DNA-binding domain was studied (the tendency of the ATPase domain to form heptamers was dominant over the dimerization function of the DNA-binding domain). However, when assembly was triggered for the full-length protein containing all three domains by using BeF_3^- to mimic phosphorylation of the regulatory receiver domain, a mixture of dimers, tetramers, and hexamers was observed (Batchelor et al., 2009). In another study of the NtrC protein of *Salmonella typhimurium*, negatively stained EM images showed that BeF_3^--activated full-length protein predominantly formed hexamer rings (De Carlo et al., 2006), but we add here that when a form of the protein able to bind DNA was activated in the presence of enhancer DNA, it formed a mixture of hexamers (83%) and heptamers (17%; S.D.C., B.T.N., and E. Nogales, unpublished data). The clear flexibility in self-assembly of these ATPases raises uncertainty about which oligomeric state or states are able to activate transcription. In this regard it may be noteworthy that virtually identical interprotomer interfaces were seen in crystal structures of heptamer and hexamer forms of the AAA+ ATPase p97 (Davies et al., 2008). For the moment, we remain mindful of such uncertainty and present the model arising from comparing the ATP- and ADP-bound crystal structures of heptamer rings as a hypothesis for further testing.

One prediction of the new model is the identity of key residues and structural changes within the Rfinger subunit that are crucial for the working cycle of the ATPase. To our knowledge these suggested roles have never been proposed despite a significant history of mutagenic studies of bEBPs. The fact that substituting K250 with glutamate gave rise to an ATPase with weakened ability to self-assemble but when assembled was able to extend GAFTGA motifs in the L1 loop and bind to σ54 (perhaps somewhat differently from the wild-type protein) indicates that the K250 residue is important for ATPase function. The further observation that adding Mg^{2+}/ADP caused this variant to precipitate but redissolve when the ADP was converted to ATP analog by the addition of BeF_x or AlF_x clearly showed that the K250 side chain experiences different environments in the ADP- and ATP-bound states, which is also a key prediction of the model.

EXPERIMENTAL PROCEDURES

Mutagenesis and Protein Purification

Mutations were made using the QuikChange Multi Site-Directed Mutagenesis Kit (Stratagene) and verified by sequencing (Penn State Nucleic Acid Facility). The $NtrC1^C$ wild-type protein and all variants containing point mutations were expressed and purified as previously described (Chen et al., 2007). His6-tagged σ54 from *Klebsiella pneumonia* was prepared as previously described (De Carlo et al., 2006).

ATP Binding and Hydrolysis

Fluorescence polarization measurements were done on a Victor3 V (Perkin Elmer) at a protein concentration of 5.3 mg/ml in buffer (20 mM Tris HCl [pH 8.0], 200 mM KCl, 2 mM $MgCl_2$). BODIPY® FL AMPPNP (Invitrogen B-22356, 100 nM) was competed away from binding sites by adding increasing amounts of ADP (200 nM–80 mM). ATP hydrolysis was measured by determining the concentration of released Pi using a heteropolyacid system as described (Chen et al., 2009b). Binding and kinetic data were analyzed using nonlinear regression via NONLIN implementations of the 4PL function or the Michaelis Menton equation, with worst-case joint confidence intervals being determined at the 67% confidence level.

ATPase Assembly and Complexation with σ54

Gel filtration chromatography was performed at room temperature using a 24 ml Superdex200 column (GE HealthCare) as described (Chen et al., 2007). Peak fractions were collected for SDS-PAGE to analyze co-elution of $NtrC1^C$ and σ54.

SAXS

Experiments were conducted on the Biophysics Collaborative Access Team (BioCAT) undulator beamline 18-ID at the Advanced Photon Source, Argonne National Laboratory (Fischetti et al., 2004) as described (Chen et al., 2007). For ab initio modeling the distance distribution function *p(R)* calculated with GNOM was used by the programs GASBOR or CREDO on the Beowolf Cluster at the University of Texas, San Antonio, to obtain 50 independent models with P7 symmetry imposed. The program SUPCOMB was used to superimpose the models and assess their similarity, and DAMAVER was used to generate the final averaged, filtered model, which was superimposed with the high-resolution crystal structure (www.embl-hamburg.de/ExternalInfo/Research/Sax/). Figures were made using Sculptor (sculptor.biomachina.org), DS Viewer (Accelrys), PyMOL (www.pymol.org), or DeepView (http://spdbv.vital-it.ch/) and PovRay (www.povray.org).

In Vitro Transcription

Open complex formation was monitored using single-round transcription assays (Xu et al., 2004). The template was supercoiled plasmid pJES535, which has the *glnA* σ54-dependent promoter upstream of a synthetic "gene" containing 7 repeats of a 21 bp module lacking T residues followed by an RNAP termination sequence.

Crystallization and Structure Determination

Crystals of E239A $NtrC1^C$ were grown at 4°C using the hanging drop vapor-diffusion method. Two microliters of protein solution (20–22 mg/ml) in base buffer (20 mM Tris [pH8.0], 200 mM KCl, and 5% glycerol) were supplemented with 5 mM TCEP, 20 mM ATP, and 5 mM $MgCl_2$, and then mixed with an equal volume of well solution containing 100 mM sodium citrate (pH 5.5), 10 mM $FeCl_3$, and 0%–5% (v/v) JeffamineM-600. Rod-shaped crystals were transferred to well solution plus 20% Jeffamine-600 and then flash frozen in liquid nitrogen for data collection at beamline 8.3.1 of the Advanced Light Source (ALS) at the Lawrence Berkeley National Laboratory. Data were processed and scaled using Crystal Clear (Rigaku). The initial phases were obtained by molecular replacement with program MrBUMP (Keegan and Winn, 2007), using the ADP-bound $NtrC1^C$ structure (PDB code: 1NY6), 140–380 residues of the subunit E. The first solution was refined by several steps of energy minimization in CNS 2.0 (Brunger et al., 1998) and by 7-fold non-crystallographic symmetry (NCS) averaging and solvent flattening. Model correction and rebuilding were accomplished with WinCoot (Emsley and Cowtan, 2004), and further improvement was achieved using PHENIX (Adams et al., 2010). During refinement NCS restraints were maintained for residues 138:214 and 220:384, hence, the difference between R_{work} and R_{free} is likely underestimated due to NCS effects. Final adjustments were made using KING (Chen et al., 2009a) based on analysis with MolProbity yielding the following statistics: clash score, 10.98 (97th percentile with N = 226, 2.63 ± 0.25 Å); rotamer outliers, 0.81%; Ramachandran outliers, 0.70%; Ramachandran favored, 96.5%; Cβ deviations > 0.25 Å, 1; MolProbity score, 1.79 (99th percentile with N = 6042, 2.63 ± 0.25 Å); bad bonds, 0; and bad angles, 0 (Davis et al., 2007).

Electron Microscopy

Samples were prepared as described (Chen et al., 2007). About 9000 particles were used for the Random Conical tilt reconstruction technique (Radermacher et al., 1987). The method was applied to the NtrC1-σ54 data set exactly as described (De Carlo et al., 2006).

ACCESSION NUMBERS

Coordinates have been deposited in the Protein Data Bank as and PDB code 3M0E.

SUPPLEMENTAL INFORMATION

Supplemental Information includes four figures, two tables, and one movie and can be found with this article online at doi:10.1016/j.str.2010.08.018.

ACKNOWLEDGMENTS

We thank Borries Demeler for facilitating our use of ATSAS software to perform ab initio modeling and averaging of SAXS data on the BCF cluster at the University of Texas Health Science Center at San Antonio, Neela Yennawar and Hemant Yennawar of the X-ray core facility at the Huck Institutes of Life Sciences, Penn State for help growing crystals and collecting initial diffraction data, and David Wemmer and Joseph Bachelor for help collecting and processing data on beamline 8.3.1 at the Advanced Light Source. The work was funded by NIH grant R01 GM069937-01A3 to B.T.N., and Use of the Advanced Photon Source was supported by the U.S. Department of Energy, Basic Energy Sciences, Office of Science, under contract no. W-31-109-ENG-38, and the Advanced Light Source is similarly supported under contract no. DE-AC02-05CH11231. BioCAT is a National Institutes of Health-supported Research Center, grant no. RR-08630. The X-ray core facility at Penn State was partially supported by NIN-NCRR grant 1S10RR023439-01. The authors declare that they have no competing financial interests.

Received: July 8, 2010
Revised: August 28, 2010
Accepted: August 30, 2010
Published: November 9, 2010

REFERENCES

Adams, P.D., Afonine, P.V., Bunkoczi, G., Chen, V.B., Davis, I.W., Echols, N., Headd, J.J., Hung, L.-W., Kapral, G.J., Grosse-Kunstleve, R.W., et al. (2010). PHENIX: a comprehensive Python-based system for macromolecular structure solution. Acta Crystallogr. D Biol. Crystallogr. *D66*, 213–221.

Batchelor, J.D., Sterling, H.J., Hong, E., Williams, E.R., and Wemmer, D.E. (2009). Receiver domains control the active-state stoichiometry of *Aquifex aeolicus* σ54 activator NtrC4, as revealed by electrospray ionization mass spectrometry. J. Mol. Biol. *393*, 634–643.

Bose, D., Pape, T., Burrows, P.C., Rappas, M., Wigneshweraraj, S.R., Buck, M., and Zhang, X. (2008). Organization of an activator-bound RNA polymerase holoenzyme. Mol. Cell *32*, 337–346.

Brunger, A.T., Adams, P.D., Clore, G.M., DeLano, W.L., Gros, P., Grosse-Kunstleve, R.W., Jiang, J.-S., Kuszewski, J., Nilges, N., Pannu, N.S., et al. (1998). Crystallography and NMR system (CNS): a new software system for macromolecular structure determination. Acta Crystallogr. D Biol. Crystallogr. *D54*, 905–921.

Chen, V.B., Davis, I.W., and Richardson, D.C. (2009a). KiNG (Kinmage, Next Generation): a versatile interactive molecular and scientific visualization program. Protein Sci. *18*, 2403–2409.

Chen, B., Doucleff, M., Wemmer, D.E., De Carlo, S., Huang, H.C., Nogales, E., Hoover, T.R., Kondrashkina, E., Guo, L., and Nixon, B.T. (2007). ATP ground- and transition states of bacterial enhancer binding AAA+ ATPases support complex formation with their target protein, σ54. Structure *15*, 429–440.

Chen, B., Sysoeva, T.A., Chowdhury, S., Guo, L., and Nixon, B.T. (2009b). ADPase activity of recombinantly expressed thermotolerant ATPases may be

caused by co-purification of adenylate kinase of *Escherichia coli*. FEBS J. *276*, 807–815.

Davies, J.M., Brunger, A.T., and Weis, W.I. (2008). Improved structures of full-length p97, an AAA ATPase: Implications for mechanisms of nucleotide-dependent conformational change. Structure *16*, 715–726.

Davis, I.W., Leaver-Fay, A., Chen, V.B., Block, J.N., Kapral, G.J., Wang, X., Murray, L.W., Arendall, W.B., III,, Snoeyink, J., Richardson, J.S., et al. (2007). MolProbity: all-atom contacts and structure validation for proteins and nucleic acids. Nucleic Acids Res. *35*, W375–W383.

De Carlo, S., Chen, B., Hoover, T.R., Kondrashkina, E., Nogales, E., and Nixon, B.T. (2006). The structural basis for regulated assembly and function of the transcriptional activator NtrC. Genes Dev. *20*, 1485–1495.

Dekker, J.P., Fodor, A., Aldrich, R.W., and Yellen, G. (2004). A perturbation-based method for calculating explicit likelihood of evolutionary co-variance in multiple sequence alignments. Bioinformatics *20*, 1565–1572.

Doucleff, M., Chen, B., Maris, A.E., Wemmer, D.E., Kondrashkina, E., and Nixon, B.T. (2005). Negative regulation of AAA+ ATPase assembly by two component receiver domains: a transcription activation mechanism that is conserved in mesophilic and extremely hyperthermophilic bacteria. J. Mol. Biol. *353*, 242–255.

Emsley, P., and Cowtan, K. (2004). Coot: model-building tools for molecular graphics. Acta Crystallogr. D Biol. Crystallogr. *D60*, 2126–2132.

Fischetti, R., Stepanov, S., Rosenbaum, G., Barrea, R., Black, E., Gore, D., Heurich, R., Kondrashkina, E., Kropf, A.J., Wang, S., et al. (2004). The BioCAT undulator beamline 18ID: a facility for biological non-crystalline diffraction and X-ray absorption spectroscopy at the Advanced Photon Source. J. Synchrotron Radiat. *11*, 399–405.

Hayward, S., and Berendsen, H.J.C. (1998). Systemic analysis of domain motions in proteins from conformational change; new results on citrate synthase and T4 lysozyme. Proteins *30*, 144–154.

Joly, N., and Buck, M. (2010). Engineered interfaces of an AAA+ ATPase reveal a new nucleotide-dependent coordination mechanism. J. Biol. Chem. *285*, 15178–15186.

Joly, N., Burrows, P.C., and Buck, M. (2008). An intramolecular route for coupling ATPase activity in AAA+ proteins for transcription activation. J. Biol. Chem. *283*, 13725–13735.

Joly, N., Schumacher, J., and Buck, M. (2006). Heterogeneous nucleotide occupancy stimulates functionality of phage shock protein F, an AAA+ transcriptional activator. J. Biol. Chem. *281*, 34997–35007.

Keegan, R.M., and Winn, M.D. (2007). Automated search-model discovery and preparation for structure solution by molecular replacement. Acta Crystallogr. D Biol. Crystallogr. *D63*, 447–457.

Kozin, M.B., and Svergun, D.I. (2001). Automated matching of high- and low-resolution structural models. J. Appl. Crystallogr. *34*, 33–41.

Lee, S.-Y., DeLaTorre, A., Yan, D., Kustu, S., Nixon, B.T., and Wemmer, D.E. (2003). Regulation of the transcriptional activator NtrC1: structural studies of the regulatory and AAA+ ATPase domains. Genes Dev. *17*, 2552–2563.

Mosca, R., and Schneider, T.R. (2008a). Alignment of protein structures in the presence of domain motions. BMC Bioinformatics *9*, 352–368.

Mosca, R., and Schneider, T.R. (2008b). RAPIDO: a web server for the alignment of protein structures in the presence of conformational changes. Nucleic Acids Res. *36*, W42–W46.

Neuwald, A.F., Aravind, L., Spounge, J.L., and Koonin, E.V. (1999). AAA+: A class of chaperonin-like ATPases associated with the assembly, operation, and disassembly of protein complexes. Genome Res. *9*, 27–43.

Radermacher, M., Wagenknecht, T., Verschoor, A., and Frank, J. (1987). Three-dimensional reconstruction from a single-exposure, random conical tilt series applied to the 50S ribosomal subunit of Escherichia coli. J. Microsc. *146*, 113–136.

Rappas, M., Schumacher, J., Beuron, F., Niwa, H., Bordes, P., Wigneshweraraj, S.R., Keetch, C.A., Robinson, C.V., Buck, M., and Zhang, X. (2005). Structural insights into the activity of enhancer-binding proteins. Science *307*, 1972–1975.

Rappas, M., Schumacher, J., Niwa, H., Buck, M., and Zhang, X. (2006). Structural basis of the nucleotide driven conformational changes in the AAA+ domain of the transcription factor PspF. J. Mol. Biol. *357*, 481–492.

Rappas, M., Bose, D., and Zhang, X. (2007). Bacterial enhancer-binding proteins: unlocking σ54-dependent gene transcription. Curr. Opin. Struct. Biol. *17*, 110–116.

Sallai, L., and Tucker, P.A. (2005). Crystal structure of the central and C-terminal domain of the sigma(54)-activator ZraR. J. Struct. Biol. *151*, 160–170.

Schumacher, J., Joly, N., Claeys-Bouuaert, I.L., Azia, S.A., Rappas, M., Zhang, X., and Buck, M. (2008). Mechanism of homotropic control to coordinate hydrolysis in a hexameric AAA+ ring ATPase. J. Mol. Biol. *381*, 1–12.

Terwilliger, T.C. (2000). Maximum likelihood density modification. Acta Crystallogr. D Biol. Crystallogr. *D56*, 965–972.

Theobald, D.L., and Wuttke, D.S. (2008). Accurate structural correlations from maximum likelihood superpositions. PLoS Comput. Biol. *4*, e43.

Thomsen, N.D., and Berger, J.M. (2008). Structural framework for considering microbial protein- and nucleic acid-dependent motor ATPases. Mol. Microbiol. *69*, 1071–1090.

Tucker, P.A., and Sallai, L. (2007). The AAA+ superfamily—a myriad of motions. Curr. Opin. Struct. Biol. *17*, 641–652.

Xu, H., Gu, B., Nixon, B.T., and Hoover, T.R. (2004). Purification and characterization of the AAA+ domain of *Sinorhizobium meliloti* DctD, a σ54-dependent transcriptional activator. J. Bacteriol. *186*, 3499–3507.

Zhang, X., and Wigley, D.B. (2008). The 'glutamate switch' provides a link between ATPase activity and ligand binding in AAA+ proteins. Nat. Struct. Mol. Biol. *15*, 1223–1227.

